RESEARCH PAPER

Just add water: reproducible singly dispersed silver nanoparticle suspensions on-demand

Robert I. MacCuspie · Andrew J. Allen ·
Matthew N. Martin · Vincent A. Hackley

Abstract Silver nanoparticles (AgNPs) are of interest due to their antimicrobial attributes, which are derived from their inherent redox instability and subsequent release of silver ions. At the same time, this instability is a substantial challenge for achieving stable long-term storage for on-demand use of AgNPs. In this study, we describe and validate a "just add water" approach for achieving suspensions of principally singly dispersed AgNPs. By lyophilizing (freeze drying) the formulated AgNPs into a solid powder, or cake, water is removed thereby eliminating solution-based chemical changes. Storing under inert gas further reduces surface reactions such as oxidation. An example of how to optimize a lyophilization formulation is presented, as well as example formulations for three AgNP core sizes. This "just add water" approach enables ease of use for the researcher desiring on-demand singly dispersed AgNP suspensions from a single master batch. Implementation of this methodology will enable studies to be performed over long periods of time and across different laboratories using particles that are identical chemically and physically and available on-demand. In addition, the approach of freeze drying and on-demand reconstitution by adding water has enabled the development of AgNP reference materials with the required shelf-life stability, one of the principal objectives of this research.

Introduction

The recent and widespread interest in the potential environmental health and safety risks of nanomaterials (nanoEHS) has included substantial work on silver nanoparticles (AgNPs) (Tolaymat et al. 2010; Fabrega et al. 2011; Meng et al. 2010; Sharma et al. 2009; Wijnhoven et al. 2009). AgNPs are of interest primarily due to their increased use in consumer products (Woodrow Wilson International Center for Scholars 2009; U.S. EPA 2012), purportedly to exploit their antimicrobial properties. Other examples include medical products (Chen and Schluesener 2008) and food packaging (Gottesman et al. 2010). The predicted growth of AgNP use in consumer products contributed to the decision by the Organization for Economic Cooperation and Development (OECD) Working Party on Manufactured Nanomaterials (WPMN) to

R. I. MacCuspie (✉) · A. J. Allen · M. N. Martin ·
V. A. Hackley
Materials Measurement Science Division, National Institute of Standards and Technology, Gaithersburg, MD 20899-8520, USA
e-mail: robert.maccuspie@nist.gov

include AgNPs as one of fourteen nanomaterials in their international testing program (OECD 2008). One of the mechanisms of antimicrobial action is believed to arise from the surface oxidation of the metallic AgNPs and subsequent dissolution into silver cations (Ag^+) (Gorham et al. 2012; Kennedy et al. 2010; Liu and Hurt 2010a; Liu et al. 2010b), which act as the active biocide (Bradford et al. 2009; Kim et al. 2009). Dissolution leads to a mass loss from the AgNPs, with subsequent changes to the size distribution (Elzey and Grassian 2010; Zook et al. 2011a), increased colloidal instability and aggregation effects, (Li et al. 2011; Lok et al. 2007; Romer et al. 2011) and potentially cycling into new "incidental" AgNPs via reduction of released silver ions (Akaighe et al. 2011; Glover et al. 2011; Maurer et al. 2012; Yin et al. 2012). Changes in size distribution, agglomeration state, and dissolved silver fraction could potentially have significance when interpreting environmental persistence or biological mechanisms of toxicity (Hussain and Schlager 2009; Levard et al. 2012; Rahman et al. 2009; Xiu et al. 2012), making long-term studies on fractions from a single suspension challenging. As a result of these many potential and likely transformations, and based on available evidence, we conclude that long-term stability of solution-phase AgNPs is an intractable issue. However, creating suspensions on-demand from AgNP powders has also proven challenging, as some frequently used commercial AgNP powders yield highly polydisperse particle distributions that are inadequate for hypothesis testing of size-based phenomena.

The instability of AgNPs obviously presents unique technical challenges for the development of AgNP reference materials, which must exhibit long-shelf life (i.e., at least 5 years) without significant changes to composition or physical properties. To increase shelf life in the pharmaceutical industry, lyophilization (or freeze drying) is frequently employed to preserve compounds, drugs, vaccines, and other biological materials (Endres et al. 2012; Lee et al. 2009; Zhang et al. 2008). Lyophilization also avoids introducing heat-related instabilities (such as AgNP dissolution) through traditional solvent-removal techniques such as rotary evaporation. Recently, lyophilization of nanoparticles has been studied systematically to explore the role that formulation and process conditions play in the lyophilization and reconstitution of nanoparticles (Abdelwahed et al. 2006; Beirowski

et al. 2011a, b, 2012; Chen and Wang 2007). Beirowski et al. have repeatedly come to the conclusion that the formulation of the nanoparticle suspension to be lyophilized is the most critical parameter to control (not the lyophilization processing conditions) when the objective is to recover the original size distribution. However, Beirowski et al. focused only on two ball-milled crystalline active pharmaceutical ingredients, leaving a critical knowledge gap for metal nanoparticles such as AgNPs.

Therefore, this study demonstrates the capacity to stabilize AgNPs for on-demand use over extended periods of time and across different laboratories. Lyophilization of AgNP suspensions, in the presence of appropriate lyophilizing agents, mitigates the risks from solution-based changes that occur on long time scales (months to years), and subsequent addition of water yields on-demand singly dispersed AgNPs. The selection of polyvinylpyrrolidone (PVP) as a combination of lyophilizing and dispersing agent is based on its inclusion in the OECD WPMN testing program on AgNPs, and on the substantial published nanoEHS literature involving PVP-capped AgNPs (Huynh and Chen 2011; Kent and Vikesland 2011; Levard et al. 2011; Lowry et al. 2012; Song et al. 2011; Stamplecoskie and Scaiano 2010; Tejamaya et al. 2012). The vacuum stoppering mechanism of the freeze drier enables backfilling with an inert gas before sealing the lyophilized material, thereby reducing further oxidative reactions. This study aims to fill the critical knowledge gap of successfully formulating freeze–dried AgNPs for the future development of reference material prototypes. Specifically, this study aims to achieve on-demand singly dispersed nanoparticle suspensions exhibiting a reproducible size distribution that reconstitutes the original (pre-lyophilization) distribution with minimal involvement by the user. Enabling the end user to just add water to the PVP–AgNP lyophilized solid (or "cake") immediately before use eliminates the variations introduced by aging, sonication (Taurozzi et al. 2012, 2011), and user-induced variability or error. The approach of freeze drying and on-demand reconstitution by just adding water offers a promising basis for the development of AgNP reference materials; toward that end, the National Institute of Standards and Technology (NIST) is currently producing RM8016, nominally 10 nm AgNPs, and RM8017, nominally 75 nm AgNPs, which will be freeze dried to extend the shelf

life of the particles over solution-based storage conditions. In addition, applications beyond reference materials could be enabled, such as providing greater flexibility for nanocomposite synthesis, where optical property control is structure dependent (Calandra et al. 2010).

Materials and methods

Preparation of PVP–AgNP lyophilized cakes

Nominally 20 nm diameter citrate-capped AgNPs were synthesized, purified, and concentrated to 1 mg mL^{-1} Ag as described elsewhere (Chinnapongse et al. 2011; MacCuspie 2011). A single batch was divided into several fractions, and then the desired amount of PVP (PVP10, Sigma-Aldrich, St. Louis, MO, USA)[1] was added to the suspension and stirred 24 h while covered with parafilm to reduce evaporation. Within 48 h, the resulting solutions were dispensed in 5.00 mL aliquots into 10 mL serum bottles for lyophilization. Samples were frozen at −20 °C for 24 h, then loaded into the vacuum stoppering adapter (Part #7593000 Labconco, Kansas City, MO, USA) and attached to a 6 L freeze drier (FreeZone 6, LabConco, Kansas City, MO, USA). One bottle had a metal thermocouple frozen into the initial aliquot to monitor the internal temperature of the solid during sublimation. Lyophilization was considered complete when the temperature of the cakes rose above the temperature of the shelf, indicating that heat was no longer being transferred from the shelf to the cake to provide the energy required to sublime the ice. Lyophilization was complete within 24 h.

For nominally 10 and 75 nm AgNPs with 40 and 10 mg mL^{-1} PVP, respectively, suspensions containing 1 mg mL^{-1}Ag were purchased from nanoComposix, Inc. (San Diego, CA, USA), stored in the dark at 4 °C, and used as received within 3 weeks of receipt. Resulting solutions were dispensed in 2.00 mL aliquots into 10 mL serum bottles for lyophilization. The samples were frozen for 3 h in the stoppering tray drier (Model 7948020, LabConco, Kansas City, MO, USA)

with a shelf temperature of −40 °C, then lyophilized for 30 h. See Fig. SI1 in the Supplementary Information (SI) for an example record of the shelf temperature, cake sample temperature, and system pressure over the course of one lyophilization run. The stoppering tray drier was backfilled with argon gas to approximately 400 Pa before the serum bottles were stoppered inside the freeze drier. Bottles were crimp sealed and stored in the dark at room temperature until reconstitution.

Instrumentation

Dynamic light scattering (DLS) was performed using a Malvern Zetasizer Nano (Westborough, MA, USA), and using disposable semi-micro UV-transparent plastic cuvettes (BrandTech, Inc., Essex, CT). A general protocol was followed to operate the DLS instrument and perform measurements (Hackley and Clogston 2007). Samples were diluted 1:100 with biological grade deionized (DI) water before measurement. DLS measurements were analyzed with both the refractive index and viscosity values of water and the refractive index and viscosity values of a PVP solution, however, at these Ag and PVP concentrations, <1 % difference in reported z-average size was found. All reported z-average diameter values are the mean of five consecutive measurements, made under repeatability conditions, with uncertainty of one standard deviation about the mean. Note, this uncertainty informs on the precision of the measurement, and is not reflective of the width of the size distribution. DLS intensity-based size distributions were obtained with Zetasizer Software v6.20 (Malvern, Westborough, MA, USA) using the general purpose analysis model.

Immediately upon completion of DLS measurements, cuvettes were transferred to a Lambda 750 Spectrophotometer (Perkin-Elmer, Waltham, MA, USA) for ultraviolet–visible (UV–vis) absorbance spectroscopy.

Atomic force microscopy (AFM) was performed on a Dimension 3100 (Bruker AXS, Santa Barbara, CA, USA), with the average height (z-displacement) of no fewer than 100 particles registered, and uncertainty of one standard deviation of the mean. Note this uncertainty is impacted by the width of the size distribution. Care was taken to minimize sample preparation-induced image artifacts, including drying-induced agglomeration (Bonevich and Haller 2010; Grobelny et al. 2009) and incidental AgNP formation (Glover

---

[1] The identification of any commercial product or trade name does not imply endorsement or recommendation by the National Institute of Standards and Technology.

et al. 2011). In brief, a 20 μL drop of suspension was placed on a 5 × 5 mm 3-aminopropyldimethylethoxysilane-functionalied Si chip for about 10 min, then rinsed with DI water for 10 s and dried using short blasts of compressed air. All AFM images were collected within 3 days of particle deposition onto the Si chip.

Ultra small angle X-ray scattering (USAXS) was performed at ChemMatCARS, sector 15-ID at the Advanced Photon Source (APS), Argonne National Laboratory, Argonne, IL, USA. The instrument is described in detail elsewhere (Allen et al. 2008; Cookson et al. 2006; Ilavsky et al. 2009b). Experiments were performed at ambient temperature (approximately 25 °C). For USAXS scans, a 0.4 × 0.4 mm monochromatic (energy = 10.5 keV, wavelength $\lambda = 0.118$ nm) incident X-ray beam was used. The scattering data were corrected for parasitic background scattering and for attenuation using data from DI water. The USAXS data, which are inherently slit-smeared perpendicular to the scanning direction, were absolute calibrated with respect to the incident beam intensity according to the first-principle methods (Ilavsky et al. 2009b), and desmeared using the Lake algorithm (Lake 1967). For measurements, two experimental setups were employed. For nominally 20 nm AgNPs, approximately 0.3 mL of suspension was enclosed within a 1-mm thick liquid cell with polyamide film windows. For nominally 10 and 75 nm AgNPs, suspensions were pumped into a nominally 1.5-mm diameter quartz capillary. To obtain quantitative nanoparticle volume fraction size distributions, the calibrated 1-D USAXS intensity data, $I(Q)$ versus Q was analyzed (where scattering vector Q has a magnitude of $Q = (4\pi/\lambda)\sin\Theta$, where λ is the X-ray wavelength and Θ is half of the scattering angle). The data were analyzed using an entropy maximization algorithm known as MaxEnt (Potton et al. 1988). The USAXS data were reduced and analyzed (including implementation of MaxEnt) within the Irena 2 package of data evaluation and modeling macros for Igor Pro (Wavemetrics, Lake Oswego, OR, USA) (Ilavsky and Jemian 2009a).

Reconstitution of lyophilized cakes

Reconstitution of lyophilized PVP–AgNP cakes involved addition of 2.00 mL of DI water, gentle shaking of the bottle by hand for approximately 1 min, and allowing the suspension to stand for 1 h under ambient laboratory light and temperature conditions before measurements. A video of this "just add water" procedure can be found in the SI.

Note all measurements reported on "stock" suspensions (i.e., suspensions that were not lyophilized) were typically collected within 48 h of the commencement of lyophilization, and always within 7 days, to compare the before- and after-lyophilization attributes of the size distributions most effectively.

Statistics

All statistical comparisons were performed in MATLAB (Natick, MA, USA) using the one-way ANOVA test with a t test to compare the individual means.

The term residual will be defined in this study as the sum of the absolute values of the differences between each data point in the size distribution, normalized to a maximum possible value of 1, yielding a unitless parameter. Residuals will be applied as a numerical assignment to estimate the difference between DLS intensity-based size distributions. The residual parameter is intended to approximate the degree of overlap between two size distributions, to provide a numerical representation of the shifts that are easy to identify visually when two size distribution plots are overlaid.

Results and discussion

Formulation optimization

When suspensions of electrostatically stabilized metal colloids (such as AgNPs) are frozen, the nanoparticles irreversibly aggregate. The freezing process forces the nanoparticles to have such a small interparticle spacing that the nanoparticles either become trapped together by attractive forces or sinter together into irregularly shaped aggregates (Albert et al. 2009). However, if sufficient repulsive force or physical barrier between NPs is present, such as through sterically bulky coatings and/or suitable lyophilizing agents, the NPs should be able to return to a singly dispersed suspension under appropriate conditions.

PVP was selected as a lyophilizing agent for reasons previously discussed. To determine the minimum concentration of PVP required to successfully

recover singly dispersed AgNPs after one lyophilization/resuspension cycle for nominally 20 nm citrate-capped AgNPs at 1.0 mg mL^{-1} total Ag, a series of formulations were examined before and after one cycle.

Visual inspection of the cakes (Fig. 1) also reveals observable differences in the lyophilized product as a function of formulation. For the smallest PVP concentrations (1 and 10 mg mL^{-1}, Fig. 1a, b), only a trace of fine black dust was observed in the bottle after lyophilization. When an optimal PVP concentration was added to the formulation (50 mg mL^{-1}, Fig. 1c), a reddish-brown cake color was observed. When excess (100 and 200 mg mL^{-1}, Fig. 1d, e) PVP was added; a yellow–brown cake color was observed.

A suite of tools, including DLS, UV–Vis, and USAXS, was employed, which were previously validated to be synergistic for characterizing AgNP aggregation phenomena (MacCuspie et al. 2011a). DLS is an excellent tool for detecting early onset of aggregation, i.e., small numbers of aggregates (Baalousha and Lead 2012; MacCuspie et al. 2011b). Figure 2 presents the DLS mean diameters for pre- and post-lyophilization suspensions (also referred to as "stock" and "reconstituted", respectively) as a function of PVP concentration for nominally 20 nm AgNPs. Insufficient PVP (≤ 10 mg mL^{-1}) leads to significant aggregation in the reconstituted suspensions, as indicated by the increased DLS diameter. However, excess amounts of PVP (≥ 100 mg mL^{-1}) result in pre-lyophilization suspensions that have a significantly increased DLS diameter, as compared to the diameter of the citrate AgNPs before the addition of the PVP. This diameter increase is likely due to an increased adsorption of PVP onto the surface of the AgNPs, creating perhaps multilayers of adsorbed PVP. Interestingly, after the lyophilization process, all the resuspended AgNPs for ≥ 50 mg mL^{-1} PVP reveal a similar DLS diameter which is consistent with the thickness of the PVP coating on the AgNPs in the pre-lyophilization 50 mg mL^{-1} PVP solution. Therefore, the excess PVP likely still provides good protection against aggregation during the lyophilization process, despite the increase in hydrodynamic size for the pre-lyophilization suspensions. This pre-lyophilization size increase could arise from either a large corona of PVP adsorbed onto the AgNPs (as mentioned above), or formation of weakly bound agglomerates that break apart during the lyophilization-reconstitution process.

DLS intensity-based size distributions provide additional insight about the recovery of the original size distribution after lyophilization. A significant increase in the size distribution occurs for the 10 mg mL^{-1} PVP formulation (Fig. 3a). For the 50 mg mL^{-1} PVP formulation (Fig. 3b), only very small shifts in the size distribution were observed, with slight increases toward larger sizes in the reconstituted
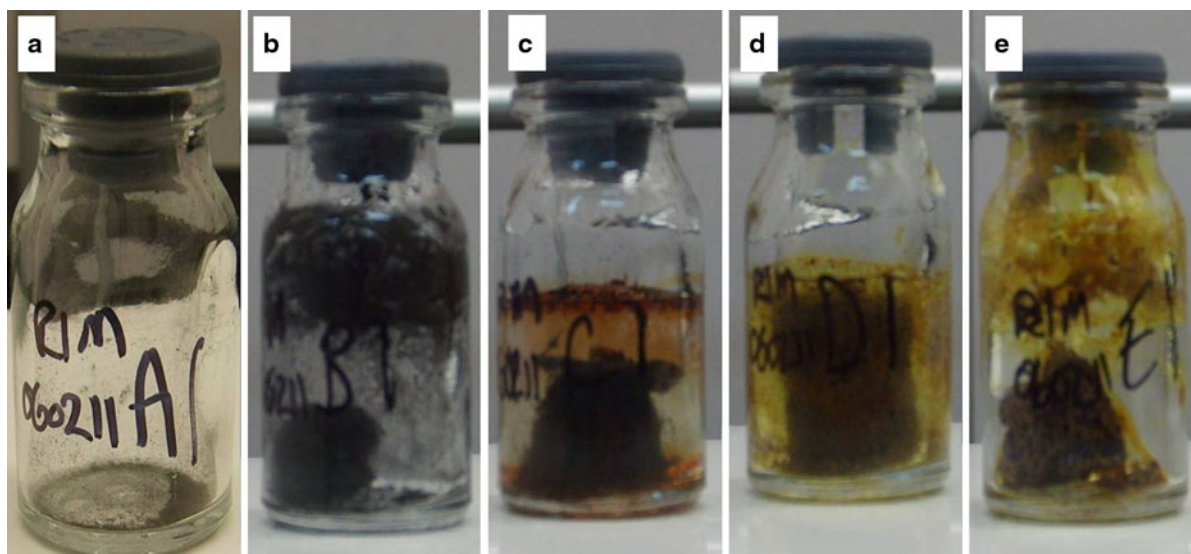
Fig. 1 *Photographs* of various lyophilized AgNP–PVP cakes. Formulations for the 20 nm AgNPs included **a** 1.0 mg mL^{-1} PVP, **b** 10 mg mL^{-1} PVP, **c** 50 mg mL^{-1} PVP, **d** 100 mg mL^{-1} PVP, and **e** 200 mg mL^{-1} PVP
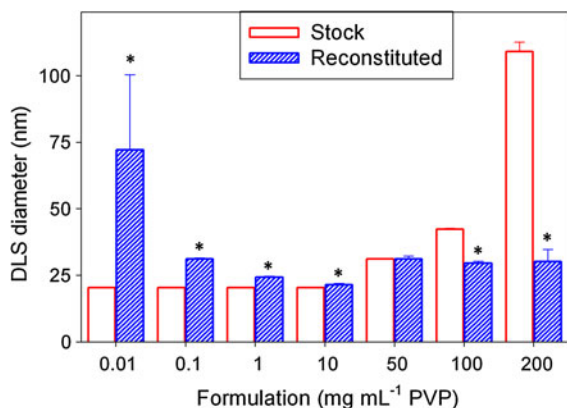
Fig. 2 DLS *z*-average (cumulants) diameter before and after one lyophilization/reconstitution cycle for the nominally 20 nm AgNPs with various PVP concentrations reported by mg mL^{-1} PVP. Data are average values from five consecutive measurements under repeatability conditions with uncertainty of one standard deviation. *Asterisks* indicate significant difference between pre-lyophilization (stock) and post-lyophilization (reconstituted) samples ($p < 0.05$)

samples. For the 100 mg mL^{-1} PVP formulation (Fig. 3c), a noticeable decrease in the size distribution was observed. The residuals were 0.68, 0.16, and 0.86 for the 100, 50, and 10 mg mL^{-1} PVP formulations, respectively. All three of these size distribution changes are also consistent with the average diameter results. While the 10 mg mL^{-1} PVP formulation does indeed provide a smaller initial and final DLS diameter compared to the 50 mg mL^{-1} PVP formulation, the 50 mg mL^{-1} PVP formulation likely has a significantly thicker shell of PVP coating the metallic AgNP core compared to the lesser PVP concentration formulations, and it is likely that the shell remains intact through the freeze drying process. Thus, it is clear that of the broad range of PVP concentrations studied by DLS, the 50 mg mL^{-1} PVP formulation provides the optimal recovery of the pre-lyophilization size distribution of the nominally 20 nm AgNPs.

USAXS provides a method to simultaneously measure the in situ size distribution and volume fraction (i.e., silver concentration) (Allen et al. 2008; Zhang et al. 2009). This enables efficient characterization for changes to the aggregation state (MacCuspie et al. 2011a), or monitoring for potential reactions (Koerner et al. 2012). When the USAXS is properly calibrated, measurement of the absolute volume fraction provides comparisons to both DLS data and UV–Vis data. USAXS is also only sensitive to the size of the silver
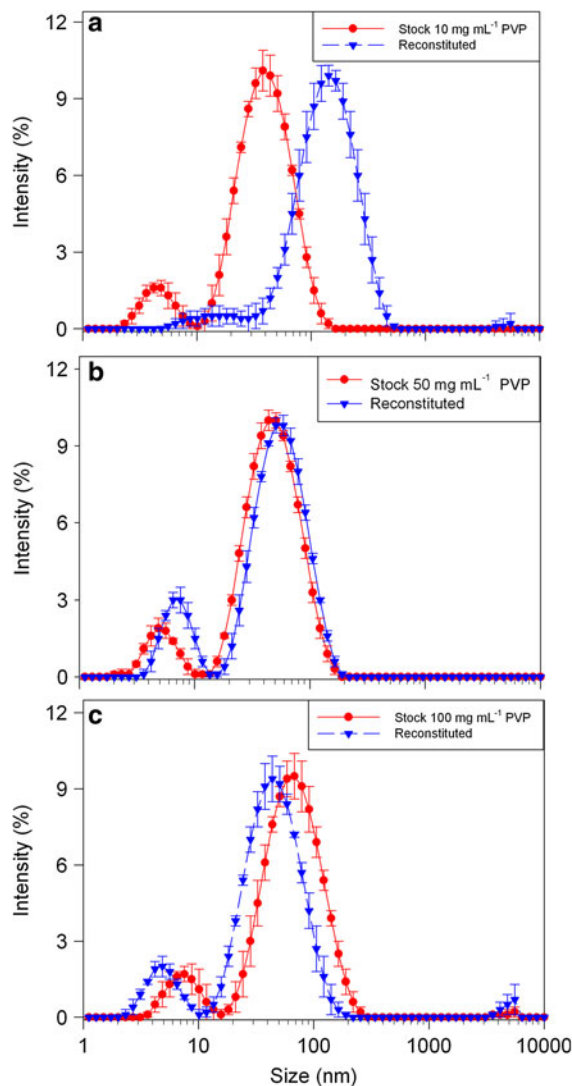
Fig. 3 DLS intensity-based size distributions for nominally 20 nm AgNPs with **a** 10 mg mL^{-1} PVP, **b** 50 mg mL^{-1} PVP, and **c** 100 mg mL^{-1} PVP formulations for the pre-lyophlization (stock, *red circles*) and post-lyophilization (reconstituted, *blue triangles*) suspensions. *Lines* are to guide the eye. (Color figure online)

metal "core" of the PVP-capped AgNPs, as the X-ray scattering cross section of the PVP corona or "shell" is negligible compared to that of silver; this provides an excellent complement to the DLS hydrodynamic size, which includes the core and attached corona.

In Fig. 4, USAXS-derived size distributions post-reconstitution for a series of formulations with nominally 20 nm AgNPs ranging from 20 to 100 mg mL^{-1} PVP are shown to determine the minimum amount of PVP required to avoid aggregation during lyophilization. This
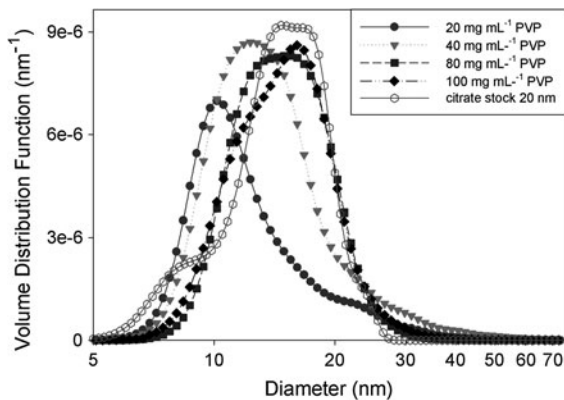
Fig. 4 USAXS derived MaxEnt volume-based size distribution functions, post-reconstitution for nominally 20 nm AgNPs for various formulations of 20–100 mg mL^{-1} PVP, and for the original citrate stock suspension. Note that the diameter (x-axis) is on a *log scale*

range was selected based upon the range identified by the DLS results. For comparison, the size distribution for the original citrate-capped AgNP suspension is also shown. The 20 mg mL^{-1} PVP formulation had incomplete recovery of the silver and a noticeable change in the shape of the size distribution. The formulations that provided the best recovery of silver and least change to the size distribution were the 40, 80, and 100 mg mL^{-1} PVP formulations. The USAXS data reveals that post-lyophilization suspensions are singly dispersed when sufficient amounts of PVP are present in the formulation. Higher levels of PVP lead to increases in the corona thickness (and therefore the hydrodynamic size), but provide the silver cores protection from aggregation. When considered together, the DLS and USAXS data reveal that, for nominally 20 nm AgNPs, 40 mg mL^{-1} PVP is the minimum formulation for a successful recovery of singly dispersed AgNPs.

Size-based observations

Three sizes of AgNP formulations were also examined in detail (Fig. 5).

Nominally 10 and 75 nm (core) AgNPs were selected, as they match the sizes chosen for the forthcoming NIST reference materials RM8016 and RM8017, as well as nominally 20 nm AgNPs synthesized in our laboratory by a commonly reported method. For the nominally 10 nm AgNPs with 40 mg mL^{-1} PVP (Fig. 5a, d, g), the mean DLS diameter remained

statistically unchanged, with values of 21.0 ± 0.5 nm for the pre-lyophilization and 20.8 ± 1.1 nm for the reconstituted post-lyophilization samples. However, slight increase to the DLS intensity-based size distribution (Fig. 5a) was observed for both the mode diameter and the width of the size distribution. It is important to note that the forthcoming NIST reference materials will provide reference values for the mean diameter by a variety of measurement techniques. It is also important to keep in mind that the repeatability and reproducibility in the mean size measurement will determine the uncertainty assigned to the reference value. Reference materials must be uniform with respect to the assigned measurand within the stated uncertainty across all units produced. Heterogeneity testing is an integral part of reference material production, as it ensures that the units comply with the stated reference values such that each unit can be utilized for quality control applications by the customer. In the present case, a broader size distribution is tolerable, since only the mean value is of consequence.

A larger DLS diameter is consistent with AFM observations (Fig. 6a, b). The height image reveals an approximately 24 nm average AgNP height for the nominally 10 nm AgNPs, however, the phase image provides an interesting insight into why there is a size difference observed between the AFM imaging and both the USAXS values (Fig. 5g) and the TEM value reported by the vendor. A very thick shell of compliant (softer) material surrounds a core of rigid (harder) material, as indicated by the dark ring surrounding the bright circular core for each of the PVP-capped AgNPs imaged by AFM. This dark ring is not observed on citrate-capped AgNPs (Fig. SI2). It is therefore worth considering that the DLS and AFM techniques are measuring the diameter of the PVP AgNPs including this thick corona of PVP adsorbed onto the AgNP surface, while techniques such as TEM and USAXS are sensitive to the metal core only. A detailed discussion of this point can be found elsewhere (MacCuspie et al. 2011b).

Absorbance spectroscopy at the surface plasmon resonance (SPR) wavelength was employed to determine if significant amounts of suspended aggregates are present. Red-shifted SPR absorbance can be easily observed from aggregates of metallic nanoparticles (Tsai et al. 2011; Zook et al. 2011b, c). The absorbance measurements of the nominally 10 nm AgNPs
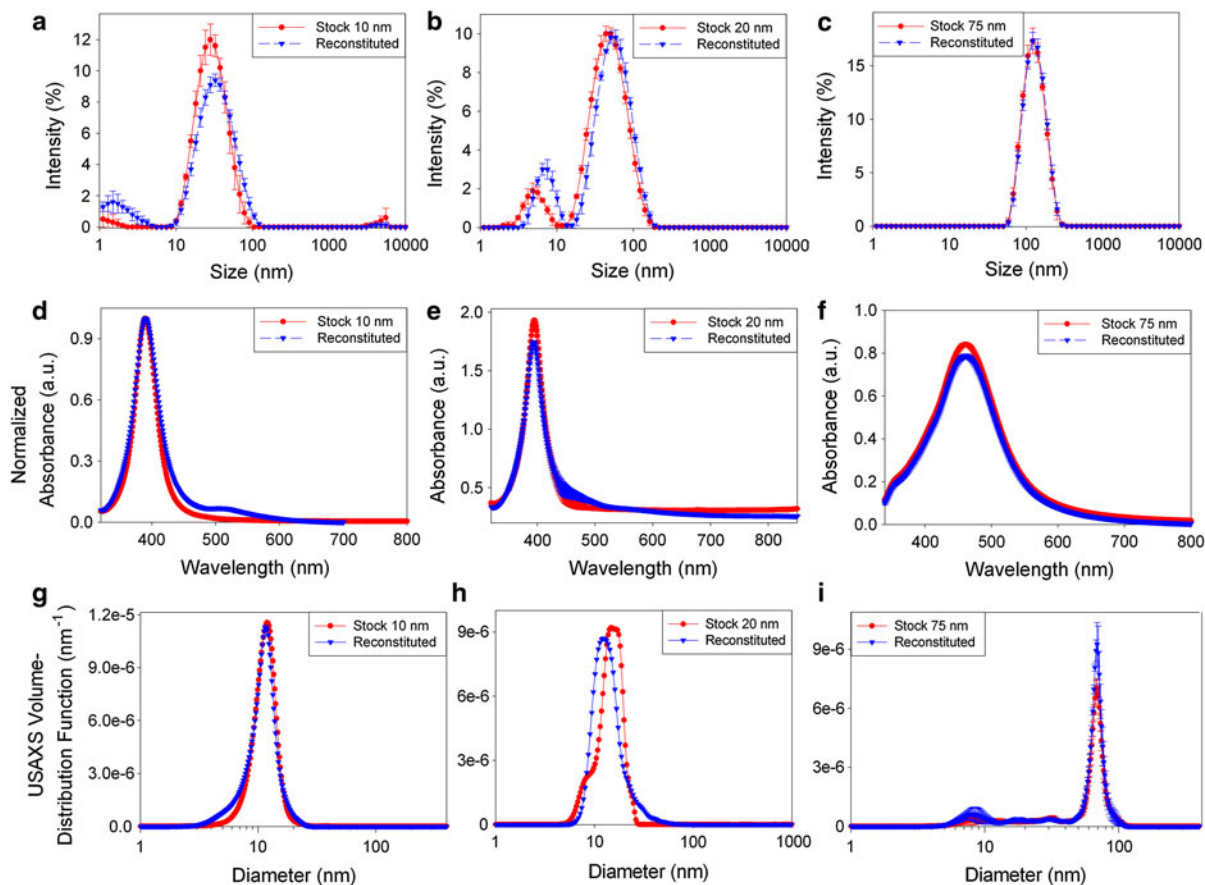
Fig. 5 DLS intensity-based size distribution *histograms* (**a–c**), absorbance spectra (**d–f**), and USAXS volume-based size distribution functions (**g–i**) of pre-lyophilization (stock, *red circles*) and post-lyophilization (reconstituted, *blue triangles*). **a**, **d**, **g** nominally 10 nm AgNPs with 40 mg mL^{-1} PVP, **b**, **e**, **h** nominally 20 nm AgNPs with **b**, **e** 50 mg mL^{-1} PVP or **h** 40 mg mL^{-1} PVP, and **c**, **f**, **i** nominally 75 nm AgNPs with 10 mg mL^{-1} PVP. DLS data are the mean of five consecutive measurements with uncertainty of one standard deviation; absorbance data are the mean of three separate sample preparations with uncertainty of one standard deviation. Uncertainties, if not visible, are smaller than the *symbols*; *lines* are to guide the eye. (Color figure online)

(Fig. 5d) suggest the presence of aggregation, with a small tail and shoulder peak at red-shifted wavelengths from the primary singly dispersed AgNP absorbance peak.

Comparing the pre- and post-lyophilization suspensions of nominally 20 nm AgNPs (Fig. 5b, e, h), only trace levels of aggregation were detectable by either DLS or absorbance measurements. As Fig. 5b is a reproduction of Fig. 3b for ease of comparison, this data have already been discussed. The absorbance spectra for the reconstituted nominally 20 nm AgNPs (Fig. 5e) reveal the appearance of a slight tail at red-shifted wavelengths. The tail is not as pronounced as the 10 nm AgNPs' shoulder peak, and thus indicates

only a very slight degree of aggregation. The overall shape of the two absorbance spectra for the nominally 20 nm AgNPs is also much more similar for the main peak, compared to the 10 nm AgNPs. The USAXS size distribution of nominally 20 nm AgNPs with a 40 mg mL^{-1} PVP formulation (Fig. 5h) reveals that the slightly polydisperse size distribution is approximately recovered after one lyophilization cycle.

For the nominally 75 nm AgNPs with a 10 mg mL^{-1} PVP formulation (Fig. 5c, f, i), a lower PVP amount was selected due to the decrease in number concentration of larger nanoparticles when the silver mass concentration remains constant. The DLS size distributions (Fig. 5f) for the pre- and post-
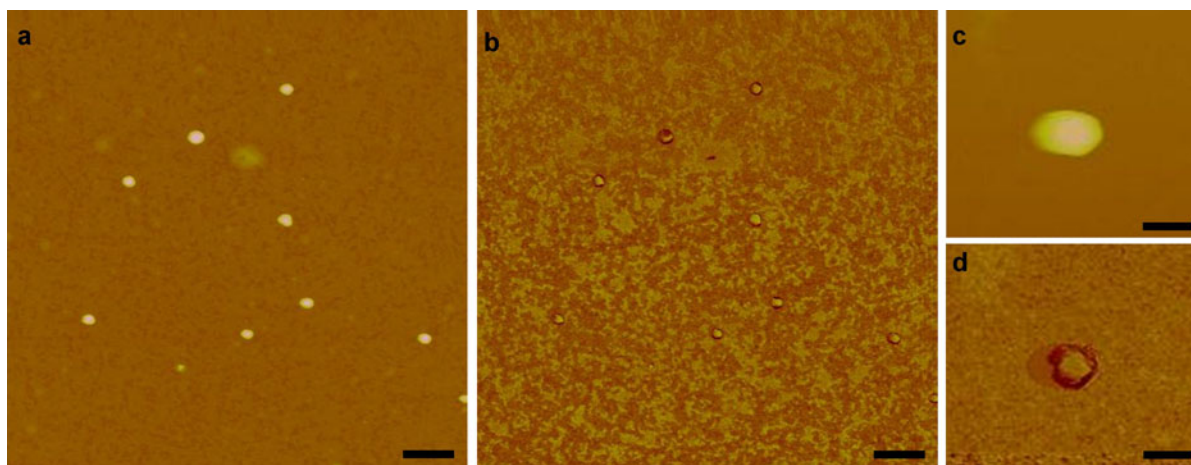
Fig. 6 AFM height (**a**, **c**) and phase (**b**, **d**) images for: **a**, **b** nominally 10 nm AgNPs with 40 mg mL^{-1} PVP and **c**, **d** nominally 75 nm AgNPs with 10 mg mL^{-1} PVP. *Scale bars* are **a**, **b** 100 nm and **c**, **d** 50 nm; *white shades* in *color scale* represent **a** 20 nm and **c** 100 nm
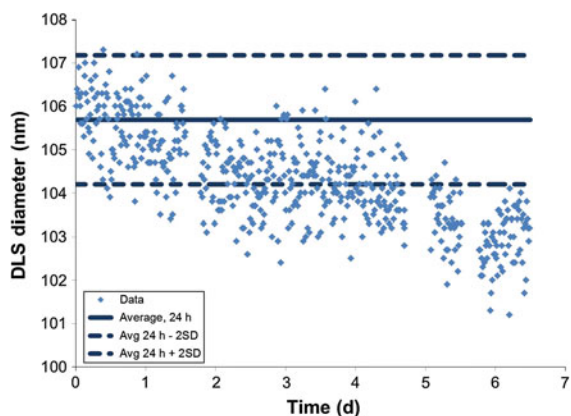
Fig. 7 DLS diameter for a reconstituted suspension diluted 1:100 in DI water and observed over 7 days. *Diamonds* represent data from individual measurements, the *thick line* represents the average of $N = 97$ DLS diameter measurements collected in the first 24 h after dilution, and the *thin lines* represent the boundaries of two standard deviations about the mean

lyophilization suspensions were identical within the uncertainty of the measurements. While the DLS diameter was larger than the nominal silver core diameter, the AFM data (Fig. 6c, d) also revealed a thick PVP corona over the silver core. In addition, Fig. 5f reveals no significant changes to the shape of the averaged absorbance spectra before and after lyophilization of nominally 75 nm AgNPs for three replicate samples, indicating recovery of the singly dispersed AgNP suspensions with no detectable aggregation. The shape of the USAXS size

distribution (Fig. 5i) is quite similar to the DLS size distribution (Fig. 5c). While the USAXS data do suggest the presence of low concentrations of small scattering objects in the reconstituted samples, unfortunately pre-lyophilization samples were not analyzed due to synchrotron beamline time constraints; additionally, the presence of small AgNPs resulting from dissolution, or as produced by measurements in electron beams has been reported by others (Bogle et al. 2006; Kent and Vikesland 2011; Kim et al. 2008). Nevertheless, the data clearly indicate the absence of detectable aggregation in the reconstituted nominally 75 nm AgNPs.

To compare the degree of aggregation by numerical differences in DLS size distributions, the residuals were again examined. For the nominally 10, 20, and 75 nm AgNPs with PVP concentrations of 40, 50, and 10 mg mL^{-1}, respectively, the residual values were 0.19, 0.16, and 0.03, respectively; recall that values of 0.68 and 0.86 were observed for nonoptimized 20 nm AgNP samples with 100 and 10 mg mL^{-1} PVP, respectively.

It is also important to note that even though the lyophilized cakes are potentially a stable way to provide long-term storage of AgNPs, after reconstitution of the freeze–dried material, the resulting aqueous suspensions are still subject to short-term changes. For example, Fig. 7 shows one of the 1:100 dilutions of the reconstituted 75 nm AgNPs observed for 7 days by DLS. The *z*-average diameter trends downward, likely due to the dilution effect causing dissociation of PVP

into solution from the thick PVP shell initially coating the AgNPs. A similar downward trend was observed in a replicate sample, and was observed to continue decreasing for 18 days of observation to a value of 99.4 ± 1.0 nm, highlighting the need to use freshly reconstituted materials to ensure consistency among experiments.

Conclusion

This study demonstrates a proof of concept for a "just add water" approach to generate on-demand suspensions of singly dispersed AgNPs from a lyophilized cake of PVP and AgNPs. A formulation for nominally 75 nm AgNPs is presented that reproduces the pre-lyophilization size distribution within the uncertainty of the measurements used. Formulations for nominally 20 and 10 nm AgNPs are presented that yield consistent size distributions from batch to batch upon reconstitution, with trace levels of aggregation in the post-lyophilization suspensions. In all cases, the lyophilized cakes were easily reconstituted by the addition of DI water, gentle shaking by hand, and allowing the suspensions to equilibrate on the bench top for 1 h. In addition, these formulations serve as prototypes for AgNP reference materials currently under development at NIST (reference materials RM8016 and RM8017). The "just add water" approach for resuspension after lyophilization and packaging under inert gas could potentially enable new classes of moderately stable nanoparticles to serve as candidates for future reference material development or for general use as test materials to assess the environmental and biological risks associated with nanoscale particles.

References

Abdelwahed W, Degobert G, Stainmesse S, Fessi H (2006) Freeze-drying of nanoparticles: formulation, process and storage considerations. Adv Drug Deliv Rev 58:1688–1713. doi:10.1016/j.addr.2006.09.017

Akaighe N, MacCuspie RI, Navarro DA, Aga DS, Banerjee S, Sohn M, Sharma VK (2011) Humic acid-induced silver nanoparticle formation under environmentally relevant conditions. Environ Sci Technol 45:2895–3901. doi:10.1021/es103946g

Albert GC, Roumeliotis M, Carson JJL (2009) The effect of temperature and freeze–thaw processes on gold nanorods. Nanotechnology 20:505502. doi:10.1088/0957-4484/20/50/505502

Allen AJ, Hackley VA, Jemian PR, Ilavsky J, Raitano JM, Chan SW (2008) In situ ultra-small-angle X-ray scattering study of the solution-mediated formation and growth of nanocrystalline ceria. J Appl Crystallogr 41:918–929. doi:10.1107/S0021889808023078

Baalousha M, Lead JR (2012) Rationalizing nanomaterial sizes measured by atomic force microscopy, flow field-flow fractionation, and dynamic light scattering: sample preparation, polydispersity, and particle structure. Environ Sci Technol 46:6134–6142. doi:10.1021/es301167x

Beirowski J, Inghelbrecht S, Arien A, Gieseler H (2011a) Freeze-drying of nanosuspensions, 1: freezing rate versus formulation design as critical factors to preserve the original particle size distribution. J Pharm Sci 100:1958–1968. doi:10.1002/jps.22425

Beirowski J, Inghelbrecht S, Arien A, Gieseler H (2011b) Freeze-drying of nanosuspensions, 2: the role of the critical formulation temperature on stability of drug nanosuspensions and its practical implication on process design. J Pharm Sci 100:4471–4481. doi:10.1002/jps.22634

Beirowski J, Inghelbrecht S, Arien A, Gieseler H (2012) Freeze-drying of nanosuspensions, part 3: investigation of factors compromising storage stability of highly concentrated drug nanosuspensions. J Pharm Sci 101:354–362. doi:10.1002/jps.22745

Bogle KA, Dhole SD, Bhoraskar VN (2006) Silver nanoparticles: synthesis and size control by electron irradiation. Nanotechnology 17:3204. doi:10.1088/0957-4484/17/13/021

Bonevich JE, Haller WK (2010) NIST–NCL joint assay protocol, PCC-7: measuring the size of nanoparticles using transmission electron microscopy (TEM). http://ncl.cancer.gov/working_assay-cascade.asp. Accessed 8 Jan 2013

Bradford A, Handy RD, Readman JW, Atfield A, Muhling M (2009) Impact of silver nanoparticle contamination on the genetic diversity of natural bacterial assemblages in estuarine sediments. Environ Sci Technol 43:4530–4536. doi:10.1021/es9001949

Calandra P, Ruggirello A, Pistone A, Liveri VT (2010) Structural and optical properties of novel surfactant coated TiO₂–Ag based nanoparticles. J Clust Sci 21:767–778. doi:10.1007/s10876-010-0330-x

Chen X, Schluesener HJ (2008) Nanosilver: a nanoproduct in medical application. Toxicol Lett 176:1–12. doi:10.1016/j.toxlet.2007.10.004

Chen G, Wang W (2007) Role of freeze drying in nanotechnology. Dry Technol 25:29–35

Chinnapongse SL, MacCuspie RI, Hackley VA (2011) Persistence of singly dispersed silver nanoparticles in natural freshwaters, synthetic seawater, and simulated estuarine waters. Sci Total Environ 409:2443–2450. doi:10.1016/j.scitotenv.2011.03.020

Cookson DJ, Kirby N, Knott R, Lee M, Schultz D (2006) Advanced photon source. Strategies for data collection and calibration on the small angle X-ray scattering camera at ChemMatCARS. J Synchrotron Radiat 13:440–444

Elzey S, Grassian V (2010) Agglomeration, isolation and dissolution of commercially manufactured silver nanoparticles in aqueous environments. J Nanopart Res 12:1945–1958

Endres T, Zheng MY, Beck-Broichsitter M, Kissel T (2012) Lyophilised ready-to-use formulations of PEG–PCL–PEI nano-carriers for siRNA delivery. Int J Pharm 428:121–124

Fabrega J, Luoma SN, Tyler CR, Galloway TS, Lead JR (2011) Silver nanoparticles: behaviour and effects in the aquatic environment. Environ Int 37:517–531

Glover RD, Miller JM, Hutchison JE (2011) Generation of metal nanoparticles from silver and copper objects: nanoparticle dynamics on surfaces and potential sources of nanoparticles in the environment. ACS Nano 5:8950–8957. doi:10.1021/nn2031319

Gorham JM, MacCuspie RI, Klein KL, Holbrook RD, Fairbrother DH (2012) UV-induced photochemical transformations of citrate-capped silver nanoparticle suspensions. J Nanopart Res 14:1139. doi:10.1007/s11051-012-1139-3

Gottesman R, Shukla S, Perkas N, Solovyov LA, Nitzan Y, Gedanken A (2010) Sonochemical coating of paper by microbiocidal silver nanoparticles. Langmuir 27:720–726. doi:10.1021/la103401z

Grobelny J, Delrio FW, Pradeep N, Kim D-I, Hackley VA, Cook RF (2009) NIST–NCL joint assay protocol, PCC-6: size measurement of nanoparticles using atomic force microscopy. http://ncl.cancer.gov/working_assay-cascade.asp. Accessed 8 Jan 2013

Hackley VA, Clogston JD (2007) NIST–NCL joint assay protocol PCC-1: measuring the size of nanoparticles in aqueous media using batch-mode dynamic light scattering. http://ncl.cancer.gov/assay_cascade.asp. Accessed 8 Jan 2013

Hussain SM, Schlager JJ (2009) Safety evaluation of silver nanoparticles: inhalation model for chronic exposure. Toxicol Sci 108:223–224

Huynh KA, Chen KL (2011) Aggregation kinetics of citrate and polyvinylpyrrolidone coated silver nanoparticles in monovalent and divalent electrolyte solutions. Environ Sci Technol 45:5564–5571. doi:10.1021/es200157h

Ilavsky J, Jemian PR (2009) Irena: tool suite for modeling and analysis of small-angle scattering. J Appl Crystallogr 42:347–353

Ilavsky J, Jemian PR, Allen AJ, Zhang F, Levine LE, Long GG (2009) Ultra-small-angle X-ray scattering at the advanced photon source. J Appl Crystallogr 42:469–479

Kennedy AJ, Hull MS, Bednar AJ, Goss JD, Gunter JC, Bouldin JL, Vikesland PJ, Steevens JA (2010) Fractionating nanosilver: importance for determining toxicity to aquatic test organisms. Environ Sci Technol 44:9571–9577. doi:10.1021/es1025382

Kent RD, Vikesland PJ (2011) Controlled evaluation of silver nanoparticle dissolution using atomic force microscopy. Environ Sci Technol 46:6977–6984. doi:10.1021/es203475a

Kim SE, Kim JU, Han YH, Lee BC, Lee JC (2008) Size controlled miniscale synthesis of silver nanoparticles using TEM electron beam. J Nanosci Nanotechnol 8:5212–5215

Kim KJ, Sung WS, Suh BK, Moon SK, Choi JS, Kim J, Lee DG (2009) Antifungal activity and mode of action of silver nano-particles on Candida albicans. Biometals 22:235–242

Koerner H, MacCuspie RI, Park K, Vaia RA (2012) In situ UV/Vis, SAXS and TEM study of single phase Au nanoparticle growth. Chem Mater 24:981–995. doi:10.1021/cm202633v

Lake JA (1967) An iterative method of slit-correcting small angle X-ray data. Acta Crystallogr 23:191–194. doi:10.1107/S0365110X67002440

Lee MK, Kim MY, Kim S, Lee J (2009) Cryoprotectants for freeze-drying of drug nano-suspensions: effect of freezing rate. J Pharm Sci 98:4808–4817

Levard C, Reinsch BC, Michel FM, Oumahi C, Lowry GV, Brown GE (2011) Sulfidation processes of PVP-coated silver nanoparticles in aqueous solution: impact on dissolution rate. Environ Sci Technol 45:5260–5266. doi:10.1021/es2007758

Levard C, Hotze EM, Lowry GV, Brown GE (2012) Environmental transformations of silver nanoparticles: impact on stability and toxicity. Environ Sci Technol 46:6900–6914. doi:10.1021/es2037405

Li X, Lenhart JJ, Walker HW (2011) Aggregation kinetics and dissolution of coated silver nanoparticles. Langmuir 28:1095–1104. doi:10.1021/la202328n

Liu J, Hurt RH (2010) Ion release kinetics and particle persistence in aqueous nano-silver colloids. Environ Sci Technol 44:2169–2175. doi:10.1021/es9035557

Liu J, Sonshine DA, Shervani S, Hurt RH (2010) Controlled release of biologically active silver from nanosilver surfaces. ACS Nano 4:6903–6913. doi:10.1021/nn102272n

Lok CN, Ho CM, Chen R, He QY, Yu WY, Sun H, Tam P, Chiu JF, Che CM (2007) Silver nanoparticles: partial oxidation and antibacterial activities. J Biol Inorg Chem 12:527–534. doi:10.1007/s00775-007-0208-z

Lowry GV, Espinasse BP, Badireddy AR, Richardson CJ et al (2012) Long-term transformation and fate of manufactured Ag nanoparticles in a simulated large scale freshwater emergent wetland. Environ Sci Technol 46:7027–7036. doi:10.1021/es204608d

MacCuspie RI (2011) Colloidal stability of silver nanoparticles with various surface coatings in biologically relevant conditions. J Nanopart Res 13:2893–2908. doi:10.1007/s11051-010-0178-x

MacCuspie RI, Allen AJ, Hackley VA (2011a) Dispersion stabilization of silver nanoparticles in synthetic lung fluid studied under in situ conditions. Nanotoxicology 5:141–157. doi:10.3109/17435390.2010.504311

MacCuspie RI, Rogers K, Patra M, Suo Z, Allen AJ, Martin MN, Hackley VA (2011b) Challenges for physical characterization of silver nanoparticles under pristine and environmentally relevant conditions. J Environ Monit 13:1212–1226. doi:10.1039/C1EM10024F

Maurer F, Christl I, Hoffmann M, Kretzschmar R (2012) Reduction and reoxidation of humic acid: influence on speciation of cadmium and silver. Environ Sci Technol. doi:10.1021/es301520s

Meng XK, Tang SC, Vongehr S (2010) A review on diverse silver nanostructures. J Mater Sci Technol 26:487–522

OECD (2008) List of manufactured nanomaterials and list of endpoints for phase one of The OECD Testing Programme. 6.

http://search.oecd.org/officialdocuments/displaydocument pdf/?cote=env/jm/mono(2010)46&doclanguage=en. Accessed 8 Jan 2013

Potton JA, Daniell GJ, Rainford BD (1988) Particle size distributions from SANS data using the maximum-entropy method. J App Cryst 21:663–668

Rahman MF, Wang J, Patterson TA, Saini UT et al (2009) Expression of genes related to oxidative stress in the mouse brain after exposure to silver-25 nanoparticles. Toxicol Lett 187:15–21

Romer I, White TA, Baalousha M, Chipman K, Viant MR, Lead JR (2011) Aggregation and dispersion of silver nanoparticles in exposure media for aquatic toxicity tests. J Chromatogr A 1218:4226–4233

Sharma VK, Yngard RA, Lin Y (2009) Silver nanoparticles: green synthesis and their antimicrobial activities. Adv Colloid Interface Sci 145:83–96

Song JE, Phenrat T, Marinakos S, Xiao Y, Liu J, Wiesner MR, Tilton RD, Lowry GV (2011) Hydrophobic interactions increase attachment of gum arabic- and PVP-coated Ag nanoparticles to hydrophobic surfaces. Environ Sci Technol 45:5988–5995. doi:10.1021/es200547c

Stamplecoskie KG, Scaiano JC (2010) Light emitting diode irradiation can control the morphology and optical properties of silver nanoparticles. J Am Chem Soc 132:1825–1827. doi:10.1021/ja910010b

Taurozzi JT, Hackley VA, Wiesner MR (2011) Ultrasonic dispersion of nanoparticles for environmental, health and safety assessment: issues and recommendations. Nanotoxicology 5:711–729. doi:10.3109/17435390.2010.528846

Taurozzi JS, Hackley VA, Wiesner MR (2012) Preparation of nanoparticle dispersions from powdered material using ultrasonic disruption. http://nvlpubs.nist.gov/nistpubs/SpecialPublications/NIST.SP.1200-2.pdf. Accessed 8 Jan 2013

Tejamaya M, Romer I, Merrifield RC, Lead JR (2012) Stability of citrate, PVP, and PEG coated silver nanoparticles in ecotoxicology media. Environ Sci Technol 46:7011–7017. doi:10.1021/es2038596

Tolaymat T, El Badawy AM, Genaidy A, Scheckel KG, Luxton TP, Suidan M (2010) An evidence-based environmental perspective of manufactured silver nanoparticle in syntheses and applications: A systematic review and critical appraisal of peer-reviewed scientific papers. Sci Total Environ 408:999–1006. doi: 10.1016/j.scitotenv.2009.11.003

Tsai DH, Cho TJ, Delrio FW, Taurozzi J, Zachariah MR, Hackley VA (2011) Hydrodynamic fractionation of finite size gold nanoparticle clusters. J Am Chem Soc 133:8884–8887

U.S. EPA (2012) Nanomaterial case study: nanoscale silver in disinfectant spray (final report). EPA/600/R-10/081F:

Wijnhoven SWP, Peijnenburg WJGM, Herberts CA, Hagens WI et al (2009) Nano-silver: a review of available data and knowledge gaps in human and environmental risk assessment. Nanotoxicology 3:109–138

Woodrow Wilson International Center for Scholars (2009) Project on emerging nanotechnologies. http://www.nanotechproject.org/inventories/consumer/analysis_draft/. Accessed 12 Mar 2010

Xiu Zm, Zhang Qb, Puppala HL, Colvin VL, Alvarez PJJ (2012) Negligible particle-specific antibacterial activity of silver nanoparticles. Nano Lett 12:4271–4275. doi:10.1021/nl301934w

Yin Y, Liu J, Jiang G (2012) Sunlight-induced reduction of ionic Ag and Au to metallic nanoparticles by dissolved organic matter. ACS Nano. doi:10.1021/nn302293r

Zhang L, Li P, Li D, Guo S, Wang E (2008) Effect of freeze–thawing on lipid bilayer-protected gold nanoparticles. Langmuir 24:3407–3411

Zhang F, Ilavsky J, Long GG, Quintana JPG, Allen AJ, Jemian PR (2009) Glassy carbon as an absolute intensity calibration standard for small-angle scattering. Metall Mater Trans A 41:1151–1158

Zook JM, Long SE, Cleveland D, Geronimo CLA, MacCuspie RI (2011a) Measuring silver nanoparticle dissolution in complex biological and environmental matrices using UV–Visible absorbance. Anal Bioanal Chem 401:1993–2002. doi:10.1007/s00216-011-5266-y

Zook JM, MacCuspie RI, Locascio LE, Halter MD, Elliott JE (2011b) Stable nanoparticle aggregates/agglomerates of different sizes and the effect of their sizes on hemolytic cytotoxicity. Nanotoxicology 5:517–530. doi:10.3109/17435390.2010.536615

Zook JM, Rastogi V, MacCuspie RI, Keene AM, Fagan J (2011c) Measuring gold nanoparticle agglomerate size distribution and dependence of localized surface plasmon resonance absorbance on agglomerate size using analytical ultracentrifugation. ACS Nano 5:8070–8079. doi:10.1021/nn202645b